

A Unified Approach for Hybrid Motion Control of MOCA Based on Weighted Whole-body Cartesian Impedance Formulation

Yuqiang Wu^{1,2}, Edoardo Lamon^{2,3}, Fei Zhao¹, Wansoo Kim², and Arash Ajoudani²

Abstract—This work presents a unified approach for hybrid motion control of the MOBILE Collaborative Robotic Assistant (MOCA). The objective is to develop a loco-manipulation controller, enabling various couplings of the arm and the mobile base movements, and particularly their purely decoupled motions. The proposed method is based on a weighted whole-body Cartesian impedance controller, where the decoupling of the motions can be achieved by solving the local optimization problem of the weighted joint torques in the first task space and its nullspace, respectively. Under this control framework, by tuning the weighting terms and a nullspace gain, three motion modes, i.e. Locomotion, Manipulation, and Modified Loco-Manipulation, are implemented. To evaluate the proposed approach, a door opening task that requires different mobility patterns of the arm, the mobile base, and their coupled movements is demonstrated. The experiment results validate the proposed methodology and provide a comprehensive understanding of the differences among the above motion modes.

Index Terms—Mobile Manipulation, Whole-Body Motion Planning and Control, Compliance and Impedance Control.

I. INTRODUCTION

THE shift from mass production to mass customization, i.e. mass production of individually customized goods and services, in industrial societies is underway. This trend increases the need for a maximum flexibility in the shop floor [1], and translates into advanced manipulation and agile locomotion capabilities of the future industrial robotic systems.

Wheeled Mobile Manipulators (WMM) are industry-suitable robotic solutions, which are usually built from a robotic manipulator (position or torque controlled) mounted on a wheeled mobile platform (velocity controlled). In terms of controller design, WMM can be considered as two separate entities or one unified system. Thus, there are mainly two control frameworks for WMM, i.e., independent and whole-body control. Under independent control, the base and the arm

This work was supported in part by the ERC-StG Ergo-Lean (Grant Agreement No.850932), in part by the National Natural Science Foundation of China under Grant 91748208, and in part by the Department of Science and Technology of Shaanxi Province under Grant 2018ZDCXL-GY-06-05. In this work, Y. Wu was also supported by the China Scholarship Council.

¹ Yuqiang Wu and Fei Zhao are with the State Key Laboratory for Manufacturing System Engineering and Shaanxi Key Laboratory of Intelligent Robots and School of Mechanical Engineering, Xi'an Jiaotong University, Xi'an Shaanxi 710049, China. wuyuqiang@stu.xjtu.edu.cn

² Yuqiang Wu, Edoardo Lamon, Wansoo Kim and Arash Ajoudani are with the Human-Robot Interfaces and physical Interaction (HRI²) group of the Istituto Italiano di Tecnologia, 16163 Genoa, Italy.

³ Edoardo Lamon is with Department of Information Engineering, Università degli Studi di Pisa, 56122 Pisa, Italy.

Digital Object Identifier (DOI): see top of this page.

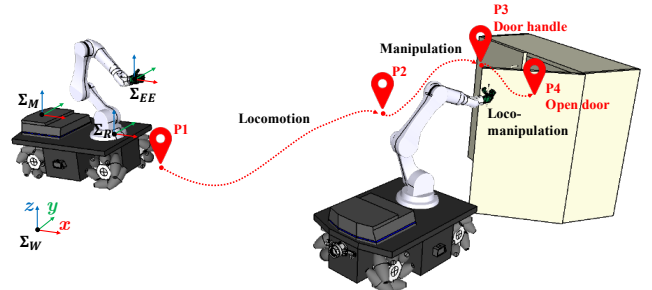


Fig. 1: A door opening task, which requires different mobility patterns of MOCA (pure locomotion and manipulation, and coupled loco-manipulation) is designed to evaluate the performance of the proposed hybrid motion controller.

exploit two independent controllers with separate reference trajectories. Although this framework has the advantage of simple and fast implementation (e.g., by exploiting the existing controllers of the two independent systems), however, it suffers from the known synchronisation problem due to the disregarded kinodynamic couplings between the two [2]. In fact, the base is less precise in kinematic planning and has slower dynamic response in comparison to the arm [3], [4].

On the other hand, under a whole-body control framework, the unified system can easily achieve a desirable motion distribution and coordination of the two [5]. For instance, the authors in [6], [7], implemented a whole-body control framework for a mobile manipulator, which was composed of a torque-controlled arm and a velocity controlled mobile base. To address this causality mismatch, an intermediate admittance controller was developed to convert the desired whole-body torque commands to the velocity references of the mobile base, while achieving the desired interaction and motion profiles at the robot end-effector. Despite the framework's interaction efficiency, in some cases, the planning problem can become complex. For instance, if the objective is to make the mobile base navigate across far distances, several constraints must be considered in the optimisation problem so that the planned end-effector trajectories would result in a desired mobile base path in a whole-body formulation [8].

To face this issue, while exploiting the redundancy of the WMM, local weighted optimization techniques can be used to regulate the control command in joint space according to the reference in Cartesian space, while fulfilling necessary constraints at the same time. When a desired velocity profile is planned, the first-order differential kinematics is used as the constraint to guarantee the joint velocity, after the local

weighted optimization procedure, replicates the desired Cartesian velocity profile [9], [10]. Similarly, if the acceleration time series are planned, the second-order differential kinematics (also known as acceleration-based formulation) [11] or the so-called torque-based formulation [12] can be used as the constraint. Towards the extension of the weighted whole-body control concept to torque-controlled mobile manipulators and Cartesian impedance control framework, in our previous work [13], a two-layer priority weighted Cartesian impedance controller was designed by formulating the problem of finding the closest control torque τ to a desired nullspace control torque τ_0 , while achieving the Cartesian impedance forces F_c at the end-effector. Although with only one optimization, the dynamically consistent weighted Jacobian transpose J_W^T and nullspace projection P_W can be found in closed form, it does not result in a completely decoupled controller, allowing for a pure locomotion or manipulation due to the existence of an identity matrix in P_W .

To address this short-coming, in this work, we propose a framework for hybrid motion control of MOCA, based on a new weighted whole-body Cartesian impedance controller. Our goal is to develop a unified motion controller for MOCA to create different mobility patterns (i.e., pure locomotion and manipulation, and coupled loco-manipulation), through appropriate selection of the weighting terms and a nullspace gain, instead of switching between different controllers as in [7]. To evaluate the proposed approach in generating different mobility patterns, a door opening task (see Fig. 1) was performed. The experiment results validated our approach, and provide a list of comparative experiments for a comprehensive understanding of the difference between the motion modes.

The remainder of this paper is structured as follows: Sec. II first briefly recaps MOCA whole-body kinematics and dynamics, after which the non-perfectly decoupled weighted nullspace projection solution in [13] is introduced. The derivation and analysis of the new weighted whole-body Cartesian impedance controller are detailed in Sec. III. Then, the experimental setup and the results are introduced and analyzed (Sec. IV). Finally, the conclusion and a short discussion is presented in Sec. V.

II. PRELIMINARIES

MOCA is a collaborative mobile manipulator, result of the integration of three main components, a Franka Emika Panda robotic arm, equipped with a underactuated Pisa/IIT SoftHand, which is mounted on top of a Robotnik SUMMIT-XL STEEL mobile platform. It was firstly introduced in our previous work [7], in which we focused more on the implementation of a teleoperation interface for loco-manipulation control. In this section, we will recap the whole-body kinematics and dynamics, and then introduce the non-perfectly decoupled weighted nullspace projection P_W [13].

A. Differential Kinematics and Dynamics of MOCA

The linear and angular velocity of the end-effector w.r.t. the world frame is the sum of the velocities resulted by the motion of the arm and the base. The whole-body Jacobian

$J_{wb} \in \mathbb{R}^{6 \times 10}$ of MOCA can be considered separately, i.e., the base and the arm, which can be formulated as:

$$\begin{bmatrix} v_{EE} \\ \omega_{EE} \end{bmatrix} = J_{wb} \dot{q} = \begin{bmatrix} J_v & J_r \end{bmatrix} \begin{bmatrix} \dot{q}_v \\ \dot{q}_r \end{bmatrix}, \quad (1)$$

where $v_{EE} \in \mathbb{R}^3$ and $\omega_{EE} \in \mathbb{R}^3$ represent the linear and angular velocities of the end effector frame Σ_{EE} w.r.t. the world frame Σ_W , respectively (see also Fig. 1). $J_v \in \mathbb{R}^{6 \times 3}$ and $J_r \in \mathbb{R}^{6 \times 7}$ respectively represent the contribution of the motion of the base and the arm. $\dot{q} = (\dot{q}_v, \dot{q}_r)^T \in \mathbb{R}^{10}$ represents whole-body joint velocity vector. $\dot{q}_v \in \mathbb{R}^3$ and $\dot{q}_r \in \mathbb{R}^7$ respectively represent the joint velocity vectors of the base and the arm.

To retrieve the whole-body dynamic model of the robot, we assume the following hypothesis [5], [7]. First, due to the high gains of the low level velocity controller, the effect of the arm motion onto the base motion are neglected, i.e. $\ddot{q}_v \approx \ddot{q}_v^{des}$, $\ddot{q}_v^{des} \in \mathbb{R}^3$ is the desired acceleration of the base. Second, the effects of the base motion onto the arm motion are reduced, thanks to the mobile base velocity limits and to the smooth trajectories generated by the planner:

$$\begin{aligned} & \begin{pmatrix} M_v & \mathbf{0} \\ \mathbf{0} & M_r \end{pmatrix} \begin{pmatrix} \ddot{q}_v \\ \ddot{q}_r \end{pmatrix} + \begin{pmatrix} D_v & \mathbf{0} \\ \mathbf{0} & C_r \end{pmatrix} \begin{pmatrix} \dot{q}_v \\ \dot{q}_r \end{pmatrix} + \begin{pmatrix} \mathbf{0} \\ g_r \end{pmatrix} \\ & = \begin{pmatrix} \tau_v \\ \tau_r \end{pmatrix} + \begin{pmatrix} \tau_v^{ext} \\ \tau_r^{ext} \end{pmatrix}, \end{aligned} \quad (2)$$

where $M_v \in \mathbb{R}^{3 \times 3}$ and $D_v \in \mathbb{R}^{3 \times 3}$ are respectively the inertial and damping set for the base in the admittance controller. $\tau_v \in \mathbb{R}^3$ and $\tau_v^{ext} \in \mathbb{R}^3$ are respectively the commanded and the external torques for the base. $M_r \in \mathbb{R}^{7 \times 7}$ is the symmetric and positive definite inertial matrix of the arm. $C_r \in \mathbb{R}^{7 \times 7}$ is the Coriolis matrix, $g_r \in \mathbb{R}^7$ is the gravity vector, $\tau_r \in \mathbb{R}^7$ and $\tau_r^{ext} \in \mathbb{R}^7$ are respectively the commanded and the external torques for the arm. For further details, please refer to [5], [7]. Moreover, thanks to the block-diagonal nature of (2), the Cartesian impedance controller design approach and stability analysis method for a redundant manipulator proposed in [14] can be extended to MOCA in a straightforward manner.

B. Non-perfectly Decoupled Weighted Nullspace Projection

The two-layer priority weighted whole-body Cartesian impedance controller was proposed in our previous work [13] in which the control algorithm was obtained by solving the following optimization problem:

$$\min_{\tau} \frac{1}{2} \|\tau - \tau_0\|_{\mathbf{W}}^2 \quad \text{s.t.} \quad \bar{J}^T \tau = F_c, \quad (3)$$

where $\mathbf{W} \in \mathbb{R}^{10 \times 10}$ is a positive definite weighting matrix. $\mathbf{M} \in \mathbb{R}^{10 \times 10}$ is the block diagonal whole-body inertia matrix. $\bar{J} = \mathbf{M}^{-1} J_{wb}^T (J_{wb} \mathbf{M}^{-1} J_{wb}^T)^{-1}$ is the dynamically consistent pseudo-inverse of J_{wb} , its transpose maps the control torques $\tau \in \mathbb{R}^{10}$ onto the operational forces $F_c \in \mathbb{R}^6$. Applying the Lagrange multipliers method, which will be explained in detail in the next section, leads to the following dynamically consistent weighted nullspace projection for the secondary task τ_0 ,

$$P_W = \mathbf{I}_{10} - \mathbf{W}^{-1} \bar{J} (\bar{J}^T \mathbf{W}^{-1} \bar{J})^{-1} \bar{J}^T. \quad (4)$$

When setting the movement priority on the arm (or base), due to the existence of the non-weighted identity matrix \mathbf{I}_{10} in \mathbf{P}_W , the resulting control torque of the base (or arm) in the secondary task space, in general, will not be zero, implying that a pure manipulation (or locomotion) cannot be achieved.

III. WEIGHTED WHOLE-BODY CARTESIAN IMPEDANCE FORMULATION

As mentioned above, the two-layer priority weighted Cartesian impedance controller proposed in [13] cannot achieve a complete decoupling of the locomotion and manipulation movements due to the existence of the non-weighted identity matrix in \mathbf{P}_W . Therefore, the objective of this work is to enable a decoupled control by considering the optimization problem separately in the first and secondary tasks space. The total control torque $\boldsymbol{\tau}$ is formulated by

$$\boldsymbol{\tau} = \boldsymbol{\tau}_t + \boldsymbol{\tau}_n = \boldsymbol{\tau}_t + \mathbf{P}_W \mathbf{K}_{vr}^n \boldsymbol{\tau}_0, \quad (5)$$

where $\boldsymbol{\tau}_t \in \mathbb{R}^{10}$ (main task) is the vector of control torques, resulted by the projection of the generalized forces \mathbf{F}_c , defined in Cartesian coordinates, and $\mathbf{K}_{vr}^n \boldsymbol{\tau}_0 \in \mathbb{R}^{10}$ is the desired secondary-task control torque vector, which after the projection to the nullspace of the first task becomes $\boldsymbol{\tau}_n \in \mathbb{R}^{10}$ (nullspace task, i.e. $\boldsymbol{\tau}_n = \mathbf{P}_W \mathbf{K}_{vr}^n \boldsymbol{\tau}_0$). $\mathbf{K}_{vr}^n \in \mathbb{R}^{10 \times 10}$ is the control gain for the secondary task.

A. Local Torque Optimization for First Task

Following [15], the optimisation problem in the first task space can be written as

$$\min_{\boldsymbol{\tau}_t} \frac{1}{2} \|\mathbf{M}^{-1} \boldsymbol{\tau}_t\|_{\mathbf{W}_t}^2 \quad \text{s.t.} \quad \bar{\mathbf{J}}^T \boldsymbol{\tau}_t = \mathbf{F}_c, \quad (6)$$

where $\mathbf{W}_t \in \mathbb{R}^{10 \times 10}$ is the positive definite weighting term for the first task. Following the method of Lagrange multipliers, (6) can be modified as

$$C(\boldsymbol{\tau}_t, \boldsymbol{\lambda}_t) = \frac{1}{2} (\mathbf{M}^{-1} \boldsymbol{\tau}_t)^T \mathbf{W}_t (\mathbf{M}^{-1} \boldsymbol{\tau}_t) + \boldsymbol{\lambda}_t^T (\mathbf{F}_c - \bar{\mathbf{J}}^T \boldsymbol{\tau}_t), \quad (7)$$

where $\boldsymbol{\lambda}_t \in \mathbb{R}^6$ is the unknown multiplier that allows the incorporation of the constraints in the cost function $C(\boldsymbol{\tau}_t, \boldsymbol{\lambda}_t)$. The solution has to satisfy the optimality conditions

$$\left(\frac{\partial C}{\partial \boldsymbol{\tau}_t} \right)^T = \mathbf{0}, \quad \left(\frac{\partial C}{\partial \boldsymbol{\lambda}_t} \right)^T = \mathbf{0}, \quad (8)$$

which lead to the following weighted solution in joint space for the control input \mathbf{F}_c in the first task space.

$$\boldsymbol{\tau}_t = \mathbf{J}_W^T \mathbf{F}_c = \mathbf{M} \mathbf{W}_t^{-1} \mathbf{M} \bar{\mathbf{J}} (\bar{\mathbf{J}}^T \mathbf{M} \mathbf{W}_t^{-1} \mathbf{M} \bar{\mathbf{J}})^{-1} \mathbf{F}_c. \quad (9)$$

B. Local Torque Optimization for Secondary Task

Thanks to the presence of redundant DoFs, a secondary task could be performed in the nullspace of the first task. The optimization problem for the secondary task can be written as following

$$\min_{\boldsymbol{\tau}_n} \frac{1}{2} \|\boldsymbol{\tau}_n - \mathbf{K}_{vr}^n \boldsymbol{\tau}_0\|_{\mathbf{W}_n^{-1}}^2 + \frac{1}{2} \|\mathbf{M}^{-1} \boldsymbol{\tau}_n\|_{\mathbf{W}_n}^2 \quad (10)$$

$$\text{s.t.} \quad \bar{\mathbf{J}}^T \boldsymbol{\tau}_n = \mathbf{0},$$

where $\mathbf{W}_n \in \mathbb{R}^{10 \times 10}$ is the secondary task weighting term. The modified cost function is formulated as

$$C(\boldsymbol{\tau}_n, \boldsymbol{\lambda}_n) = \frac{1}{2} (\boldsymbol{\tau}_n - \mathbf{K}_{vr}^n \boldsymbol{\tau}_0)^T \mathbf{W}_n^{-1} (\boldsymbol{\tau}_n - \mathbf{K}_{vr}^n \boldsymbol{\tau}_0) + \frac{1}{2} (\mathbf{M}^{-1} \boldsymbol{\tau}_n)^T \mathbf{W}_n (\mathbf{M}^{-1} \boldsymbol{\tau}_n) - \boldsymbol{\lambda}_n^T \bar{\mathbf{J}}^T \boldsymbol{\tau}_n. \quad (11)$$

Following the same procedure as in the previous section in (8), the solution for secondary task is retrieved as

$$\boldsymbol{\tau}_n = (\mathbf{I}_w^{-1} - \mathbf{I}_w^{-1} \mathbf{W}_n \bar{\mathbf{J}} (\bar{\mathbf{J}}^T \mathbf{I}_w^{-1} \mathbf{W}_n \bar{\mathbf{J}})^{-1} \bar{\mathbf{J}}^T \mathbf{I}_w^{-1}) \mathbf{K}_{vr}^n \boldsymbol{\tau}_0, \quad (12)$$

where $\mathbf{I}_w = \mathbf{I}_{10} + \mathbf{W}_n \mathbf{M}^{-1} \mathbf{W}_n \mathbf{M}^{-1} \in \mathbb{R}^{10 \times 10}$. Compared with the solution (4), solution (12) presents a weighted identity matrix \mathbf{I}_w which plays a crucial role to implement the decoupled control of the arm and base in the secondary task space. The optimisation problem in (10) includes two sub-cost functions. The first one is used to optimize $\boldsymbol{\tau}_n$ to reach $\mathbf{K}_{vr}^n \boldsymbol{\tau}_0$ to the extent possible. The second shares the same structure with (6), which is used to distribute a weighted control torque for the secondary task. Noteworthy, the weighting term used in the first sub-cost function is the inverse of the weighting term used in the second sub-cost function. The purpose of this setting is to avoid any conflict between these two sub-cost functions. To explain this better, assume that both sub-cost functions use a high weighting term for a particular joint. In the first sub-cost function, this would imply that the resulting nullspace control torque in that joint must get as close as possible to the corresponding element in $\mathbf{K}_{vr}^n \boldsymbol{\tau}_0$. However, in the second sub-cost function, this would result in the minimisation of the nullspace control torque for that joint, to the maximum extent possible, which will be in conflict with the former. Hence, the introduction of the inverse of the weighting term in the first sub-cost function is to avoid such a conflict.

C. Further Analysis by Decomposing Weighting Terms

To generate arm, mobile base, or coupled motions through (5), the weighting terms \mathbf{W}_t and \mathbf{W}_n should be properly selected. In [16], the inertia matrix has been chosen as the weighting term which fulfills the dynamically consistent projection condition and the corresponding inverse minimizes the instantaneous kinetic energy of the robotic system. Based on this study, we consider a diagonal weighting matrix $\mathbf{S} \in \mathbb{R}^{10 \times 10}$ alongside the inertia matrix to formulate \mathbf{W}_t and \mathbf{W}_n , i.e., $\mathbf{W}_t = \mathbf{S} \mathbf{M}$ and $\mathbf{W}_n = \sqrt{\mathbf{S}} \mathbf{M}$ which are similar with the choice in [13]. In the following, $\boldsymbol{\tau}_t$ and $\boldsymbol{\tau}_n$ are decomposed as

$$\boldsymbol{\tau}_t = \begin{bmatrix} \boldsymbol{\tau}_t^v \\ \boldsymbol{\tau}_t^r \end{bmatrix}, \quad \boldsymbol{\tau}_n = \begin{bmatrix} \boldsymbol{\tau}_n^v \\ \boldsymbol{\tau}_n^r \end{bmatrix}, \quad (13)$$

where $\boldsymbol{\tau}_t^v \in \mathbb{R}^3$ and $\boldsymbol{\tau}_t^r \in \mathbb{R}^7$ represent the commanded torques for the base and the arm respectively, generated by the first task. $\boldsymbol{\tau}_n^v \in \mathbb{R}^3$ and $\boldsymbol{\tau}_n^r \in \mathbb{R}^7$ are the commanded torques for the base and the arm respectively, to fulfill the second task. For the first task, we can separate $\mathbf{W}_t = \mathbf{S} \mathbf{M}$ into two blocks corresponding to the mobile base and the robotic arm, respectively

$$\mathbf{W}_t = \mathbf{S} \mathbf{M} = \begin{bmatrix} \mathbf{S}_v \mathbf{M}_v & \mathbf{0} \\ \mathbf{0} & \mathbf{S}_r \mathbf{M}_r \end{bmatrix}, \quad (14)$$

where $\mathbf{S}_v \in \mathbb{R}^{3 \times 3}$ and $\mathbf{S}_r \in \mathbb{R}^{7 \times 7}$ respectively represent the diagonal weighting matrices for the base and the arm. By substituting (14), the definition of dynamically consistent Jacobian $\bar{\mathbf{J}} = \mathbf{M}^{-1} \mathbf{J}^T \mathbf{\Lambda}$, and re-writing $\mathbf{\Lambda} = (\mathbf{\Lambda}_v^{-1} + \mathbf{\Lambda}_r^{-1})^{-1}$, the weighted control torques for the base and the arm in (9) become

$$\begin{bmatrix} \boldsymbol{\tau}_t^v \\ \boldsymbol{\tau}_t^r \end{bmatrix} = \begin{bmatrix} \mathbf{S}_v^{-1} \mathbf{J}_v^T (\mathbf{\Lambda}_{wv}^{-1} + \mathbf{\Lambda}_{wr}^{-1})^{-1} (\mathbf{\Lambda}_v^{-1} + \mathbf{\Lambda}_r^{-1}) \\ \mathbf{S}_r^{-1} \mathbf{J}_r^T (\mathbf{\Lambda}_{wv}^{-1} + \mathbf{\Lambda}_{wr}^{-1})^{-1} (\mathbf{\Lambda}_v^{-1} + \mathbf{\Lambda}_r^{-1}) \end{bmatrix} \mathbf{F}_c \quad (15)$$

where $\mathbf{\Lambda}_{wv} \in \mathbb{R}^{6 \times 6}$ and $\mathbf{\Lambda}_{wr} \in \mathbb{R}^{6 \times 6}$ are respectively the weighted Cartesian inertia of the base and the arm which are formulated as following:

$$\mathbf{\Lambda}_{wv} = (\mathbf{J}_v \mathbf{M}_v^{-1} \mathbf{S}_v^{-1} \mathbf{J}_v^T)^{-1}, \quad (16)$$

$$\mathbf{\Lambda}_{wr} = (\mathbf{J}_r \mathbf{M}_r^{-1} \mathbf{S}_r^{-1} \mathbf{J}_r^T)^{-1}. \quad (17)$$

$\mathbf{\Lambda}_v \in \mathbb{R}^{6 \times 6}$ and $\mathbf{\Lambda}_r \in \mathbb{R}^{6 \times 6}$ are respectively the actual (non-weighted) Cartesian inertia of the base and the arm which can be formulated by setting $\mathbf{S}_v = \mathbf{I}_v$ and $\mathbf{S}_r = \mathbf{I}_r$, where $\mathbf{I}_v \in \mathbb{R}^{3 \times 3}$ and $\mathbf{I}_r \in \mathbb{R}^{7 \times 7}$ are identity matrices.

For the secondary task, we can write

$$\mathbf{W}_n = \sqrt{\mathbf{S}} \mathbf{M} = \begin{bmatrix} \sqrt{\mathbf{S}_v} \mathbf{M}_v & \mathbf{0} \\ \mathbf{0} & \sqrt{\mathbf{S}_r} \mathbf{M}_r \end{bmatrix}. \quad (18)$$

Hence, the control torques for the base and the arm are

$$\begin{bmatrix} \boldsymbol{\tau}_n^v \\ \boldsymbol{\tau}_n^r \end{bmatrix} = \mathbf{P}_W \mathbf{K}_{vr}^n \boldsymbol{\tau}_0 = \begin{bmatrix} \mathbf{P}_W^v & \mathbf{P}_W^{vr} \\ \mathbf{P}_W^r & \mathbf{P}_W^r \end{bmatrix} \mathbf{K}_{vr}^n \boldsymbol{\tau}_0, \quad (19)$$

where $\mathbf{P}_W \in \mathbb{R}^{10 \times 10}$ is the dynamically consistent weighted nullspace projection. The sub matrices $\mathbf{P}_W^v \in \mathbb{R}^{3 \times 3}$, $\mathbf{P}_W^{vr} \in \mathbb{R}^{3 \times 7}$, $\mathbf{P}_W^r \in \mathbb{R}^{7 \times 3}$ and $\mathbf{P}_W^r \in \mathbb{R}^{7 \times 7}$ are formulated as follows according to (12):

$$\begin{aligned} \mathbf{P}_W^v &= \mathbf{I}_{S_v}^{-1} - \mathbf{I}_{S_v}^{-1} \sqrt{\mathbf{S}_v} \mathbf{J}_v^T (\mathbf{\Lambda}_{wv}^{*-1} + \mathbf{\Lambda}_{wr}^{*-1})^{-1} \mathbf{J}_v \mathbf{M}_v^{-1} \mathbf{I}_{S_v}^{-1}, \\ \mathbf{P}_W^{vr} &= -\mathbf{I}_{S_v}^{-1} \sqrt{\mathbf{S}_v} \mathbf{J}_v^T (\mathbf{\Lambda}_{wv}^{*-1} + \mathbf{\Lambda}_{wr}^{*-1})^{-1} \mathbf{J}_r \mathbf{M}_r^{-1} \mathbf{I}_{S_r}^{-1}, \\ \mathbf{P}_W^r &= -\mathbf{I}_{S_r}^{-1} \sqrt{\mathbf{S}_r} \mathbf{J}_r^T (\mathbf{\Lambda}_{wv}^{*-1} + \mathbf{\Lambda}_{wr}^{*-1})^{-1} \mathbf{J}_r \mathbf{M}_r^{-1} \mathbf{I}_{S_r}^{-1}, \\ \mathbf{P}_W^r &= \mathbf{I}_{S_r}^{-1} - \mathbf{I}_{S_r}^{-1} \sqrt{\mathbf{S}_r} \mathbf{J}_r^T (\mathbf{\Lambda}_{wv}^{*-1} + \mathbf{\Lambda}_{wr}^{*-1})^{-1} \mathbf{J}_v \mathbf{M}_v^{-1} \mathbf{I}_{S_v}^{-1}. \end{aligned} \quad (20)$$

where $\mathbf{I}_{S_v} \in \mathbb{R}^{3 \times 3}$, $\mathbf{I}_{S_r} \in \mathbb{R}^{7 \times 7}$, $\mathbf{\Lambda}_{wv}^* \in \mathbb{R}^{6 \times 6}$ and $\mathbf{\Lambda}_{wr}^* \in \mathbb{R}^{6 \times 6}$ are formulated as following

$$\mathbf{I}_{S_v} = \mathbf{I}_v + \mathbf{S}_v, \quad \mathbf{I}_{S_r} = \mathbf{I}_r + \mathbf{S}_r, \quad (21)$$

$$\mathbf{\Lambda}_{wv}^* = (\mathbf{J}_v \mathbf{M}_v^{-1} \mathbf{I}_{S_v}^{-1} \sqrt{\mathbf{S}_v} \mathbf{J}_v^T)^{-1}, \quad (22)$$

$$\mathbf{\Lambda}_{wr}^* = (\mathbf{J}_r \mathbf{M}_r^{-1} \mathbf{I}_{S_r}^{-1} \sqrt{\mathbf{S}_r} \mathbf{J}_r^T)^{-1}. \quad (23)$$

D. Motion Control Modes

Under the new weighted whole-body Cartesian impedance controller, and through the scaling of the weighting terms \mathbf{S}_v and \mathbf{S}_r , besides the Classical Loco-Manipulation (CLM) motion mode developed in [5], [7], Locomotion (L) and Manipulation (M) are introduced. Furthermore, by distinguishing \mathbf{S}_v as $\mathbf{S}_v^t \in \mathbb{R}^{3 \times 3}$ and $\mathbf{S}_v^n \in \mathbb{R}^{3 \times 3}$ respectively corresponding to the first task weighting term and secondary task weighting term of the mobile base, a Modified Loco-Manipulation (MLM) control mode is constructed. The difference between CLM and MLM is that in the first task space, the movement

priority is set on the arm in MLM while it is set equal for the arm and base in CLM. All the motion modes and their corresponding weighting terms are summarised in Tab. I with α, β and $\gamma \rightarrow \infty$. Infinite weighting term means the movement priority is set on the other component. To make the effects of the weighting terms visible, Fig. 2 illustrates the priority set for the arm and the base in first and secondary tasks space in different motion modes.

TABLE I: MOCA Motion Mode Parameter Settings

Motion Mode	\mathbf{S}_v^t	\mathbf{S}_v^n	\mathbf{S}_r
CLM	\mathbf{I}_v	\mathbf{I}_v	\mathbf{I}_r
Locomotion	\mathbf{I}_v	\mathbf{I}_v	$\alpha \times \mathbf{I}_r$
Manipulation	$\beta \times \mathbf{I}_v$	$\beta \times \mathbf{I}_v$	\mathbf{I}_r
MLM	$\gamma \times \mathbf{I}_v$	\mathbf{I}_v	\mathbf{I}_r

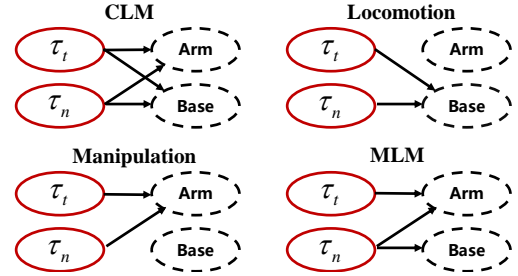


Fig. 2: In CLM, the priority is set equal for the arm and base in both first and secondary tasks; In Locomotion, the priority is set on the base in both first and secondary tasks while in Manipulation, the priority is set on the arm in both first and secondary tasks; In MLM, for the first task, the priority is set on the arm while it is set equal for the arm and base for the secondary task.

In the following, The resulted controller formulation for each motion mode is derived by replacing the weighting terms by the corresponding values listed in Tab. I.

1) *CLM*: For Classical Loco-Manipulation control mode [5], \mathbf{S}_v and \mathbf{S}_r are selected as identity matrices. Thus (15) and (19) become

$$\begin{bmatrix} \boldsymbol{\tau}_t^v \\ \boldsymbol{\tau}_t^r \end{bmatrix} = \begin{bmatrix} \mathbf{J}_v^T \\ \mathbf{J}_r^T \end{bmatrix} \mathbf{F}_c, \quad (24)$$

$$\begin{bmatrix} \boldsymbol{\tau}_n^v \\ \boldsymbol{\tau}_n^r \end{bmatrix} = \begin{bmatrix} \mathbf{I}_v - \mathbf{J}_v^T \mathbf{\Lambda} \mathbf{J}_v \mathbf{M}_v^{-1} & -\mathbf{J}_v^T \mathbf{\Lambda} \mathbf{J}_r \mathbf{M}_r^{-1} \\ -\mathbf{J}_r^T \mathbf{\Lambda} \mathbf{J}_v \mathbf{M}_v^{-1} & \mathbf{I}_r - \mathbf{J}_r^T \mathbf{\Lambda} \mathbf{J}_r \mathbf{M}_r^{-1} \end{bmatrix} \frac{\mathbf{K}_{vr}^n \boldsymbol{\tau}_0}{2}, \quad (25)$$

where $\mathbf{\Lambda} = (\mathbf{\Lambda}_v^{-1} + \mathbf{\Lambda}_r^{-1})^{-1}$.

2) *Locomotion*: To implement the Locomotion control mode, we can set $\mathbf{S}_v = \mathbf{I}_v$, $\mathbf{S}_r = \alpha \times \mathbf{I}_r$ with $\alpha \rightarrow \infty$. Hence, $\mathbf{S}_r^{-1} \rightarrow \mathbf{0}$, $\mathbf{I}_{S_r}^{-1} \rightarrow \mathbf{0}$ and $\mathbf{I}_{S_r}^{-1} \sqrt{\mathbf{S}_r} \rightarrow \mathbf{0}$, leads to a pure locomotion using (15) and (19):

$$\begin{bmatrix} \boldsymbol{\tau}_t^v \\ \boldsymbol{\tau}_t^r \end{bmatrix} = \begin{bmatrix} \mathbf{J}_v^T (\mathbf{I}_6 + \mathbf{\Lambda}_v \mathbf{\Lambda}_r^{-1}) \\ \mathbf{0} \end{bmatrix} \mathbf{F}_c, \quad (26)$$

$$\begin{bmatrix} \boldsymbol{\tau}_n^v \\ \boldsymbol{\tau}_n^r \end{bmatrix} = \begin{bmatrix} \mathbf{I}_v - \mathbf{J}_v^T \mathbf{\Lambda}_v \mathbf{J}_v \mathbf{M}_v^{-1} & \mathbf{0} \\ \mathbf{0} & \mathbf{0} \end{bmatrix} \frac{\mathbf{K}_{vr}^n \boldsymbol{\tau}_0}{2}. \quad (27)$$

3) *Manipulation*: On the other hand, to implement the Manipulation mode, we can set $\mathbf{S}_r = \mathbf{I}_r$, $\mathbf{S}_v = \beta \times \mathbf{I}_v$, with $\beta \rightarrow \infty$. Thus, $\mathbf{S}_v^{-1} \rightarrow \mathbf{0}$, $\mathbf{I}_{S_v}^{-1} \rightarrow \mathbf{0}$ and $\mathbf{I}_{S_v}^{-1} \sqrt{\mathbf{S}_v} \rightarrow \mathbf{0}$, the same structured equations as the above can be derived

$$\begin{bmatrix} \boldsymbol{\tau}_t^v \\ \boldsymbol{\tau}_t^r \end{bmatrix} = \begin{bmatrix} \mathbf{0} \\ \mathbf{J}_r^T (\mathbf{I}_6 + \mathbf{\Lambda}_r \mathbf{\Lambda}_v^{-1}) \end{bmatrix} \mathbf{F}_c, \quad (28)$$

$$\begin{bmatrix} \tau_n^v \\ \tau_n^r \end{bmatrix} = \begin{bmatrix} \mathbf{0} & \mathbf{0} \\ \mathbf{I}_r - \mathbf{J}_r^T \mathbf{\Lambda}_r \mathbf{J}_r \mathbf{M}_r^{-1} & \frac{\mathbf{K}_{vr}^n \tau_0}{2} \end{bmatrix}. \quad (29)$$

4) *MLM*: Under Modified Loco-Manipulation control mode, the weighting terms are set as following: $\mathbf{S}_v^t = \gamma \times \mathbf{I}_v$, with $\gamma \rightarrow \infty$, $\mathbf{S}_v^n = \mathbf{I}_v$ and $\mathbf{S}_r = \mathbf{I}_r$. The controller formulations for the first and secondary tasks are respectively

$$\begin{bmatrix} \tau_t^v \\ \tau_t^r \end{bmatrix} = \begin{bmatrix} \mathbf{0} \\ \mathbf{J}_r^T (\mathbf{I}_6 + \mathbf{\Lambda}_r \mathbf{\Lambda}_v^{-1}) \end{bmatrix} \mathbf{F}_c, \quad (30)$$

$$\begin{bmatrix} \tau_n^v \\ \tau_n^r \end{bmatrix} = \begin{bmatrix} \mathbf{I}_v - \mathbf{J}_v^T \mathbf{\Lambda}_v \mathbf{J}_v \mathbf{M}_v^{-1} & -\mathbf{J}_v^T \mathbf{\Lambda}_v \mathbf{J}_r \mathbf{M}_r^{-1} \\ -\mathbf{J}_r^T \mathbf{\Lambda}_v \mathbf{J}_v \mathbf{M}_v^{-1} & \mathbf{I}_r - \mathbf{J}_r^T \mathbf{\Lambda}_v \mathbf{J}_r \mathbf{M}_r^{-1} \end{bmatrix} \frac{\mathbf{K}_{vr}^n \tau_0}{2}. \quad (31)$$

It is important to note here that, in Locomotion mode, for MOCA, the maximum rank of \mathbf{J}_v is three (since there are only three DoFs available in the mobile base). Hence, the calculation of $\mathbf{\Lambda}_v$ in (26) and (27), may suffer from singularity problems. Furthermore, referring to the difference in the actuation/control of the arm (torque-controlled) and the base (velocity controlled), zero torque commands would generate zero velocity profiles through the admittance controller for the base, keeping it motionless. However, zero torque commands for the arm would result in a gravity compensated arm (the arm's gravity is compensated by its inner controller), which is unfavourable when navigating in an environment (since rapid base movements might cause arm motions). More importantly, the Cartesian impedance control law implemented in the first task space in general manages the translational and rotational impedance relationship along three orthogonal directions which means at least six DoFs is necessary to reach the desired behavior for the controller. Otherwise, the system could behave like under actuated which happens in Locomotion mode. Considering the above problems in Locomotion mode, instead of using (26) and (27), the Locomotion mode can be implemented based on the Classical Loco-Manipulation control mode but with a higher arm nullspace gain, which results in an approximately fixed arm configuration of the arm, while enabling robot navigation in space.

In summary, based on the unified weighted whole-body Cartesian impedance controller, the final and suitable values of the weighting terms and nullspace gain \mathbf{K}_{vr}^n settings of all the above motion modes are summarised in Tab. II and all the motion modes will be evaluated in our experiments.

TABLE II: MOCA Motion Mode Parameter Settings

Motion Mode	\mathbf{S}_v^t	\mathbf{S}_v^n	\mathbf{S}_r	\mathbf{K}_{vr}^n
CLM	\mathbf{I}_v	\mathbf{I}_v	\mathbf{I}_r	$100 \times \mathbf{I}_{10}$
Locomotion	\mathbf{I}_v	\mathbf{I}_v	\mathbf{I}_r	$200 \times \mathbf{I}_{10}$
Manipulation	$1000 \times \mathbf{I}_v$	$1000 \times \mathbf{I}_v$	\mathbf{I}_r	$100 \times \mathbf{I}_{10}$
MLM	$1000 \times \mathbf{I}_v$	\mathbf{I}_v	\mathbf{I}_r	$100 \times \mathbf{I}_{10}$

IV. EXPERIMENTS AND RESULTS

A typical door opening task, which requires different motion patterns of MOCA, i.e., locomotion, manipulation, and loco-manipulation, is considered in this study. As depicted in Fig. 1, the closet is far from the starting point (P1), where MOCA is

initially placed. The off-line planned actions for the MOCA robot is to pass from P2, reach P3 and grasp the door handle of the closet, open the door, and eventually stop at P4. The proposed controller was running on a 8-cores Intel Core i7-8GB RAM computer with 1 kHz control loop.

According to the distance-based motion mode selection principle proposed by [17], the door open task was divided into three phases: (1) locomotion phase (from point P1 to P2) performed by the Locomotion mode; (2) manipulation phase (from point P2 to P3) performed by Manipulation mode; and (3) loco-manipulation phase (from point P3 to P4) performed by Modified Loco-Manipulation mode. The motion mode for each phase was predefined and autonomously switched to the next one according to a Finite State Machine (FSM). A sigmoid function was used to guarantee a smooth transition between different motion modes. In our experiments, MOCA was controlled by the weighted whole-body Cartesian impedance controller and the control input τ_0 in the secondary task space was generated by functions of arm manipulability optimization and joint limitation avoidance, as explained in the following.

To extend the optimisation problem of the arm manipulability [18], to mobile manipulators (hence to exploit additional DoFs of the mobile base in optimising the arm manipulability), we consider an infinitesimal displacement $\Delta \mathbf{Q}_M \in \mathbb{R}^6$ of the mobile base local frame Σ_M in the secondary task space, $\Delta \mathbf{Q}_M$ leading to an infinitesimal displacement $\Delta \mathbf{q}_r \in \mathbb{R}^7$ in the joint space of the arm. From a relative motion point of view, they are related by (32) in which the Moore-Penrose inverse is used for calculating the inverse of arm Jacobian and the appearance of $\mathbf{S}(\mathbf{r}_{m,r})$ is due to the fact that for most mobile manipulators, the base frame Σ_R of the arm does not coincide with the local frame Σ_M of the mobile robot.

$$\Delta \mathbf{q}_r = -\mathbf{J}_r^+ \begin{bmatrix} \mathbf{I}_3 & -\mathbf{S}(\mathbf{r}_{m,r}) \\ \mathbf{0} & \mathbf{I}_3 \end{bmatrix} \Delta \mathbf{Q}_M, \quad (32)$$

where $\mathbf{r}_{m,r} \in \mathbb{R}^3$ represents the vector from the origin of Σ_M to the origin of Σ_R represented in Σ_W . $\mathbf{S}(\mathbf{r}_{m,r}) \in \mathbb{R}^{3 \times 3}$ is the skew symmetric matrix.

Then in the secondary task, the control torque $\tau_m \in \mathbb{R}^6$ of the base for the arm manipulability optimization can be calculated numerically by:

$$\begin{aligned} \tau_m &= \frac{\text{Manip}(\mathbf{Q}_M + \Delta \mathbf{Q}_M) - \text{Manip}(\mathbf{Q}_M - \Delta \mathbf{Q}_M)}{2\Delta \mathbf{Q}_M} \\ &= \frac{\text{Manip}(\mathbf{q}_r + \Delta \mathbf{q}_r) - \text{Manip}(\mathbf{q}_r - \Delta \mathbf{q}_r)}{2\Delta \mathbf{Q}_M}. \end{aligned} \quad (33)$$

In our experiment, the ratio $\frac{\sigma_{min}}{\sigma_{max}} \in \mathbb{R}$ between the minimum ($\sigma_{min} \in \mathbb{R}$) and maximum ($\sigma_{max} \in \mathbb{R}$) singular values of the translational part of \mathbf{J}_r^R was used as the manipulability index $\text{Manip}()$ (see [18] for the definition of manipulability index).

For the joint limits avoidance of the arm, (34) was used to measure the distance from mechanical joint limits

$$\omega(\mathbf{q}_r) = -\frac{1}{2n} \sum_{i=1}^n \left(\frac{q_{ri} - \bar{q}_{ri}}{q_{ri,M} - q_{ri,m}} \right)^2, \quad (34)$$

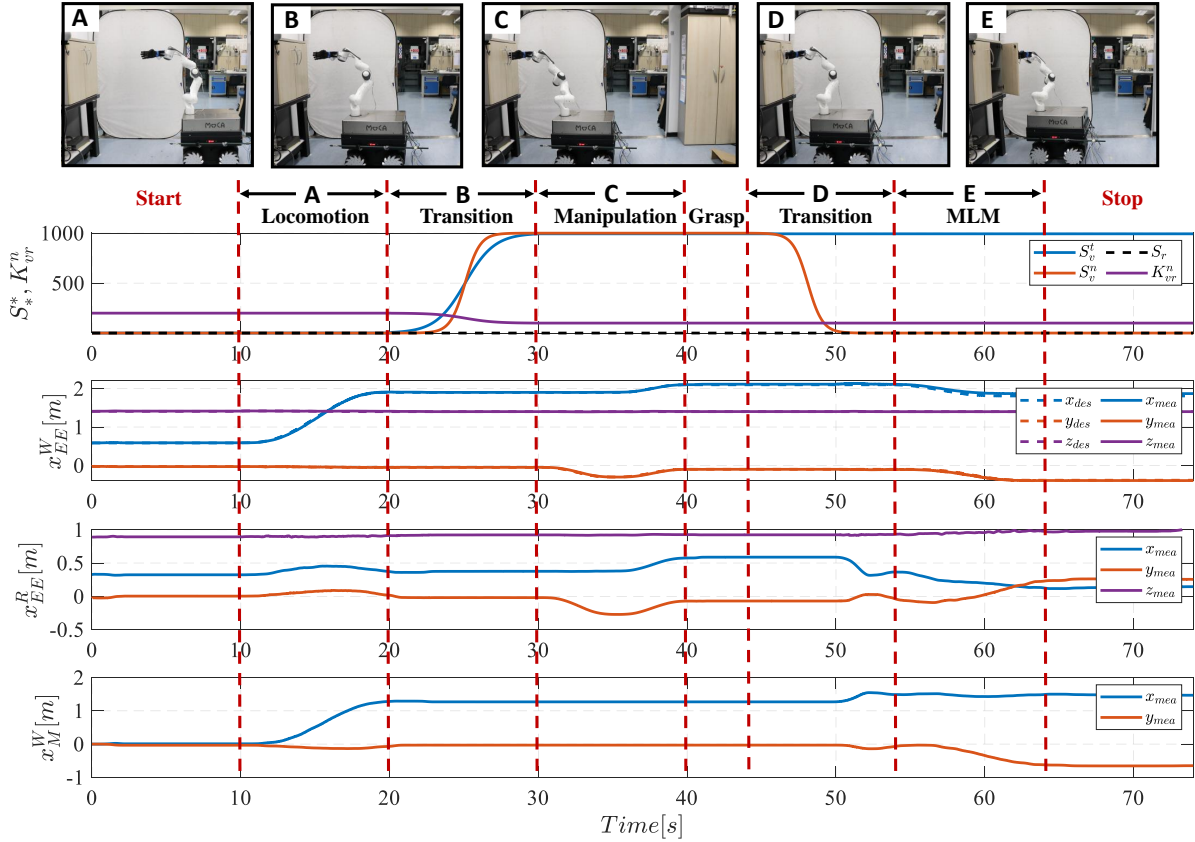


Fig. 3: Starting with the Locomotion mode, the base navigated 1.312m in x direction (indicated by A). Next, the controller transitioned to the Manipulation mode smoothly (indicated by B). In the next phase, the base kept still and the arm was commanded to reach the door handle precisely (indicated by C). The Pisa/IIT SoftHand was used to grasp the door handle. After a transition from Manipulation to MLM mode (indicated by D), the door opening task was finished by taking advantage of the coordinated motion from the base and arm (indicated by E).

TABLE III: Constant Controller Parameters for the Experiments

Parameters	Value
M_v	$diag(40kg, 40kg, 8kg \cdot m^2)$
D_v	$diag(128kg/s, 128kg/s, 25.6kg \cdot m^2/s)$
K_{tra}	$diag(600N/m, 600N/m, 600N/m)$
K_{rot}	$diag(30Nm/rad, 30Nm/rad, 30Nm/rad)$
D_{imp}	$\xi = (0.7, 0.7, 0.7, 0.7, 0.7, 0.7)$

where $n = 7$ and the differentiation of $\omega(\mathbf{q}_r) \in \mathbb{R}$ w.r.t. arm joint variables was used to contribute to τ_0 . $q_{ri,M}$ ($q_{ri,m}$) denotes the maximum (minimum) limit of i -th joint of the arm and \bar{q}_{ri} is the middle value of the joint range. Except for the weighting terms and nullspace gain values listed in Tab. II, other parameters in the controller under different motion modes were kept the same as in Tab. III. $K_{tra} \in \mathbb{R}^{3 \times 3}$ and $K_{rot} \in \mathbb{R}^{3 \times 3}$ are respectively the translational and the rotational stiffness set for the weighted whole-body Cartesian impedance controller. The damping matrix $D_{imp} \in \mathbb{R}^{6 \times 6}$ is configuration-dependent, which is implemented based on the Double Diagonalization design in [19], to achieve the damping ratios $\xi \in \mathbb{R}^6$.

The experiment results are provided in Fig. 3. The entire process to finish the typical door opening task is defined by *start* \rightarrow *Locomotion* \rightarrow *transition* \rightarrow *Manipulation* \rightarrow *grasp* \rightarrow *transition* \rightarrow *Modified Loco-Manipulation* \rightarrow *stop*. The Locomotion mode first received the desired trajectory

of moving forward 1.312 m. As it is observable from the end-effector position $\mathbf{x}_{EE}^W \in \mathbb{R}^3$ w.r.t. to Σ_W , $\mathbf{x}_{EE}^R \in \mathbb{R}^3$ w.r.t. to Σ_R and the base position $\mathbf{x}_M^W \in \mathbb{R}^2$ w.r.t. to Σ_W in Fig. 3, the movement was performed by the mobile base in the locomotion phase (indicated by A). Subsequently, a smooth transition (indicated by B) was executed to transfer from Locomotion mode to Manipulation mode. The desired trajectory in manipulation phase was performed by the arm only (indicated by C), as it can be observed from the variations of \mathbf{x}_M^W , \mathbf{x}_{EE}^W and \mathbf{x}_{EE}^R . This was followed by a grasping action, after which, a transition (indicated by D) was performed to transfer from Manipulation mode to MLM mode, to initiate the door opening action. During this transition, since the secondary task control torque τ_n^v for the base was not zero any longer, $\frac{\sigma_{min}}{\sigma_{max}}$ and $\omega(\mathbf{q})$ of the arm were further optimized by taking advantage of the movements of the base which can be seen from the video in attachment, available also in <https://youtu.be/3fFygViV-kA>. Finally, with the coupled motion of the base and the arm, the door open task was executed (indicated by E) using MLM mode.

To provide a comprehensive understanding of all motion control modes, a comparison study was demonstrated between different motion modes in each phase, as explained hereafter. For the locomotion task, besides the Locomotion mode, CLM or MLM modes can be exploited (Manipulation mode is not considered due to the fact that in general, for locomotion

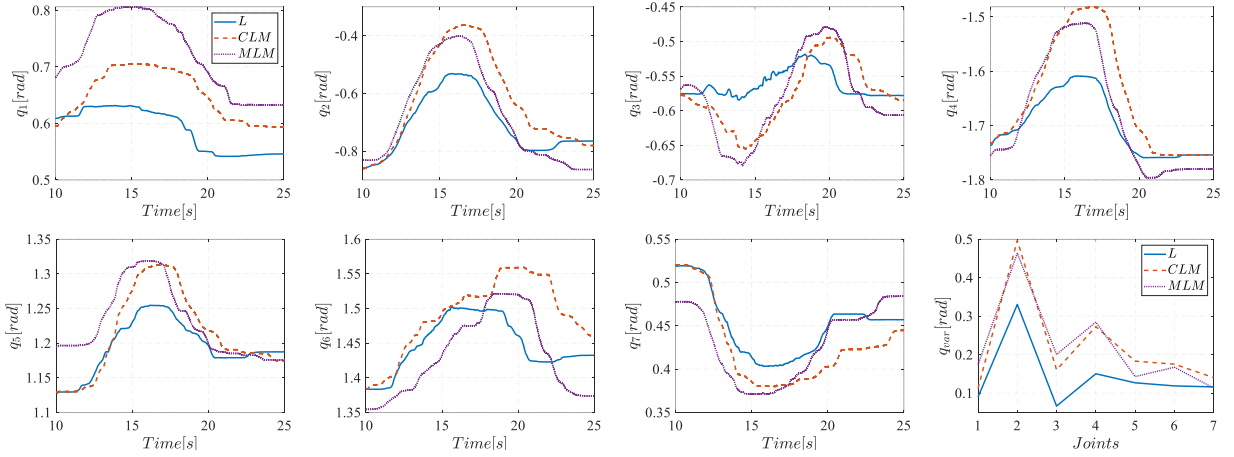


Fig. 4: Comparisons of the variations of arm joint angles between Locomotion (L), CLM and MLM motion modes for performing locomotion phase. The last subplot shows the variation ranges from the first joint to the last joint of the arm. All joints moved less in Locomotion mode than the other two, especially the second, third and fourth joints due to the configuration of the arm.

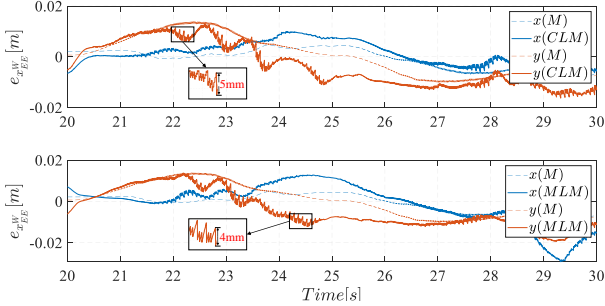


Fig. 5: Comparisons of the end-effector tracking errors between Manipulation (M), CLM and MLM for performing manipulation phase. Blue and red lines are respectively for x and y directions. The tracking errors under Manipulation mode (dashed lines) were less fluctuated and noisy than those under CLM and MLM modes. The noise amplitudes for CLM and MLM were respectively 5mm and 4mm which limit their use in accurate manipulation applications.

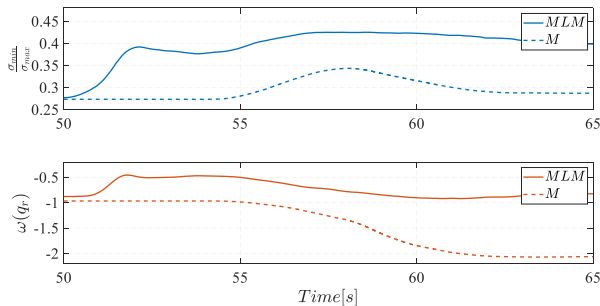


Fig. 6: Comparisons of $\frac{\sigma_{min}}{\sigma_{max}}$ and $\omega(\mathbf{q}_r)$ between MLM and Manipulation (M) when performing loco-manipulation phase. In MLM motion mode, the base is also used to do the optimization in secondary task space which outperforms the optimization behavior only with the arm in M mode.

tasks, the target position is out of the workspace of the arm). Fig. 4 illustrates the variations of the arm joint angles under different motion control modes (solid blue line is the result by using Locomotion mode, dashed red and purple lines are respectively the results by using CLM and MLM). To measure the variability of joint angles, The variation range of each arm joint was depicted in the last subplot of Fig. 4. As seen in the

plots, all the arm joints moved less in Locomotion mode than the other two motion modes, especially the second, third and fourth joints due to the configuration of the arm. According to the above results, it could be concluded that compared with CLM and MLM, Locomotion control mode, which uses a higher K_{vr}^n is more effective than the other two.

For the manipulation task, although base movement is not desirable when manipulating close to constraint environments, CLM and MLM modes were also implemented (Locomotion mode is not considered due to the fact that in general, Locomotion control mode has less DoFs to perform manipulation tasks) in our experiment. As shown in Fig. 5, the end-effector tracking errors (blue lines for x direction and red lines for y direction) between Manipulation (dashed lines), CLM (solid lines on the top) and MLM (solid lines on the bottom) control modes were compared. Although the magnitudes of the tracking errors performed by the above three modes did not show significant difference, the tracking errors under manipulation mode were less fluctuated and much less noisy than the results under CLM and MLM control modes. The noise amplitudes for CLM and MLM were respectively 5mm and 4mm in the experiment which limit their use in accurate manipulation applications.

For the loco-manipulation phase, besides the MLM mode, Manipulation and CLM control modes were adopted for performing the door opening task. Since the door opening action requires a relatively large motion range of the end-effector, it could result in arm singularity, mechanical joint limitation, or even a collision with the door, which happened in our experiment. As shown in Fig. 6, under Manipulation mode, $\frac{\sigma_{min}}{\sigma_{max}}$ (dashed blue line) and $\omega(\mathbf{q}_r)$ (dashed red line) were much lower than the corresponding indexes (blue and red solid lines, respectively) under MLM mode due to the fact that in MLM mode, the base was also used to do the optimization which is supposed to outperform the optimization behavior only with the arm in Manipulation mode. Compared with MLM mode which sets priority on the arm in the first task space, CLM sets equal priority on the arm and base. When the robot's end-effector interacts with the environment with

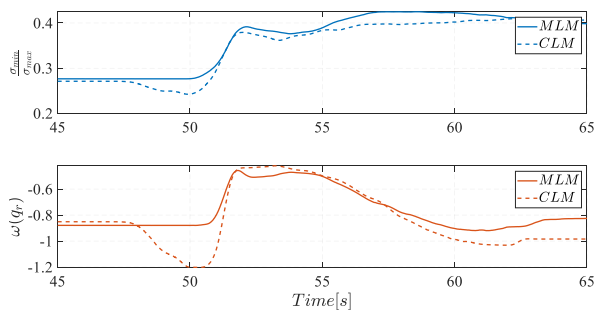


Fig. 7: Comparisons of $\frac{\sigma_{min}}{\sigma_{max}}$ and $\omega(\mathbf{q}_r)$ between MLM and CLM when performing loco-manipulation phase. Due to the large interaction forces applied to the door handle after the grasping at around 50s, $\frac{\sigma_{min}}{\sigma_{max}}$ and $\omega(\mathbf{q}_r)$ significantly reduced in CLM mode.

large forces, they may degrade the behavior of the robot in the secondary task space to a great extent. After the grasping action, MOCA’s end-effector applied large interaction forces to the door handle, resulting in unexpected movement of the base in the CLM control mode. As shown in Fig. 7, $\frac{\sigma_{min}}{\sigma_{max}}$ and $\omega(\mathbf{q}_r)$ indexes significantly reduced at around 50s in CLM mode. After this period, the interaction forces decreased during the coordinated loco-manipulation movement, while opening the door. However, for continuously interactive tasks, MLM can outperform CLM due to the fact that in general the arm responds faster than the base, and in the MLM control mode, the secondary task will be least affected by the first task.

V. CONCLUSION AND DISCUSSION

In this work, we proposed a unified approach for hybrid motion control of our Mobile Collaborative Robot Assistant (MOCA). The method is based on weighted whole-body Cartesian impedance control, which is implemented by exploiting local optimization techniques of weighted joint torques. Under the weighted whole-body control framework, by tuning the weighting terms and the nullspace gain, besides the Classical Loco-Manipulation motion mode, three extra motion modes are developed, i.e., Locomotion, Manipulation and Modified Loco-Manipulation. To evaluate the proposed approach, a door opening task that requires various motion patterns of MOCA was demonstrated. The experimental results validated our approach and provided a comprehensive understanding of the difference among the above motion modes.

Although the results with MOCA shows the method outperforms state-of-the-art methods, it has two main limitations. First, the derivation of the weighted whole-body Cartesian impedance controller and its stability analysis rely on the decoupled dynamics assumption between the arm and base. In our platform, we can assume this thanks to the hypothesis in Sec. II-A. For robots that do not present such property, the control algorithm can be applied only if the coupling terms are pre-compensated, such as in [6]. Second, in Locomotion mode only 3 DoFs are controllable for MOCA. In such cases, the Cartesian impedance control law allow to achieve only a pose in $SE(2)$ (coordinates x, y and yaw). Hence, it is not possible to impose an arbitrary motion to the end-effector in $SE(3)$.

Overall, the method can be applied to highly redundant robots with a torque control interface and multiple kinematic chains characterized by different dynamics. In case of some velocity or position controlled kinematic chains, it is possible to embed an admittance interface to map high-level torques into low-level velocity/position commands. Finally, it is important to highlight that, in case of legged robots, the approach should be modified to ensure stability at first task and all the others in the redundant space.

REFERENCES

- [1] S. Bogh, C. Schou, T. Rühr, Y. Kogan, A. Dömel, M. Brucker, C. Eberst, R. Tornese, C. Sprunk, G. D. Tipaldi *et al.*, “Integration and assessment of multiple mobile manipulators in a real-world industrial production facility,” in *ISR/Robotik 2014; 41st International Symposium on Robotics*, 2014, pp. 1–8.
- [2] L.-P. Ellekilde and H. I. Christensen, “Control of mobile manipulator using the dynamical systems approach,” in *2009 IEEE International Conference on Robotics and Automation*. IEEE, 2009, pp. 1370–1376.
- [3] D. H. Shin, B. S. Hamner, S. Singh, and M. Hwangbo, “Motion planning for a mobile manipulator with imprecise locomotion,” in *Proceedings 2003 IEEE/RSJ International Conference on Intelligent Robots and Systems*, vol. 1. IEEE, 2003, pp. 847–853.
- [4] Y. Yamamoto and X. Yun, “Coordinating locomotion and manipulation of a mobile manipulator,” *IEEE Transactions on Automatic Control*, vol. 39, no. 6, pp. 1326–1332, 1994.
- [5] A. Dietrich, T. Wimböck, and A. Albu-Schäffer, “Dynamic whole-body mobile manipulation with a torque controlled humanoid robot via impedance control laws,” in *2011 IEEE/RSJ International Conference on Intelligent Robots and Systems*. IEEE, 2011, pp. 3199–3206.
- [6] A. Dietrich, K. Bussmann, F. Petit, P. Kotyczka, C. Ott, B. Lohmann, and A. Albu-Schäffer, “Whole-body impedance control of wheeled mobile manipulators,” *Autonomous Robots*, vol. 40, no. 3, pp. 505–517, 2016.
- [7] Y. Wu, P. Balatti, M. Lorenzini, F. Zhao, W. Kim, and A. Ajoudani, “A teleoperation interface for loco-manipulation control of mobile collaborative robotic assistant,” *IEEE Robotics and Automation Letters*, vol. 4, no. 4, pp. 3593–3600, 2019.
- [8] A. Dietrich and C. Ott, “Hierarchical impedance-based tracking control of kinematically redundant robots,” *IEEE Transactions on Robotics*, vol. 36, no. 1, pp. 204–221, 2019.
- [9] T. F. Chan and R. V. Dubey, “A weighted least-norm solution based scheme for avoiding joint limits for redundant joint manipulators,” *IEEE Transactions on Robotics and Automation*, vol. 11, 1995.
- [10] M. Mashali, “Kinematic control of redundant mobile manipulators,” *Ph.D. dissertation*, 2015.
- [11] S. Ma, S. Hirose, and D. N. Nenchev, “Improving local torque optimization techniques for redundant robotic mechanisms,” *Journal of Robotic Systems*, vol. 8, no. 1, pp. 75–91, 1991.
- [12] S. Ma, “Local torque optimization of redundant manipulators in torque-based formulation,” in *Proceedings of IECON’94-20th Annual Conference of IEEE Industrial Electronics*, vol. 2. IEEE, 1994, pp. 697–702.
- [13] E. Lamon, M. Leonori, W. Kim, and A. Ajoudani, “Towards an intelligent collaborative robotic system for mixed case palletizing,” in *2020 IEEE International Conference on Robotics and Automation (ICRA)*, 2020, pp. 9128–9134.
- [14] C. Ott, *Cartesian impedance control of redundant and flexible-joint robots*. Springer, 2008.
- [15] F. Flacco and A. De Luca, “Discrete-time redundancy resolution at the velocity level with acceleration/torque optimization properties,” *Robotics and Autonomous Systems*, vol. 70, pp. 191–201, 2015.
- [16] O. Khatib, “A unified approach for motion and force control of robot manipulators: The operational space formulation,” *IEEE Journal on Robotics and Automation*, vol. 3, no. 1, pp. 43–53, 1987.
- [17] P. Ferrari, M. Cagnetti, and G. Oriolo, “Humanoid whole-body planning for loco-manipulation tasks,” in *2017 IEEE International Conference on Robotics and Automation (ICRA)*. IEEE, 2017, pp. 4741–4746.
- [18] T. Yoshikawa, “Manipulability of robotic mechanisms,” *The international journal of Robotics Research*, vol. 4, no. 2, pp. 3–9, 1985.
- [19] A. Albu-Schaffer, C. Ott, U. Frese, and G. Hirzinger, “Cartesian impedance control of redundant robots: Recent results with the dlr-light-weight-arms,” in *2003 IEEE International Conference on Robotics and Automation*, vol. 3. IEEE, 2003, pp. 3704–3709.